"Smart" Base Isolation Systems

J. C. Ramallo[1]; E. A. Johnson, A.M.ASCE[2]; and B. F. Spencer Jr., M.ASCE[3]

Abstract: A "smart" base isolation strategy is proposed and shown to effectively protect structures against extreme earthquakes without sacrificing performance during the more frequent, moderate seismic events. The proposed smart base isolation system is composed of conventional low-damping elastomeric bearings and "smart" controllable (semiactive) dampers, such as magnetorheological fluid dampers. To demonstrate the advantages of this approach, the smart isolation system is compared to lead-rubber bearing isolation systems. The effectiveness of the isolation approaches are judged based on computed responses to several historical earthquakes scaled to various magnitudes. The limited performance of passive systems is revealed and the potential advantages of smart dampers are demonstrated. Two- and six-degree-of-freedom models of a base-isolated building are used as a test bed in this study. Smart isolation is shown to achieve notable decreases in base drifts over comparable passive systems with no accompanying increase in base shears or in accelerations imparted to the superstructure. In contrast to passive lead-rubber bearing systems, the adaptable nature of the smart damper isolation system provides good protection to both the structure and its contents over a wide range of ground motions and magnitudes.

Introduction

One of the most widely implemented and accepted seismic protection systems is base isolation. Seismic base isolation (Skinner et al. 1993; Naeim and Kelly 1999) is a technique that mitigates the effects of an earthquake by essentially *isolating* the structure and its contents from potentially dangerous ground motion, especially in the frequency range where the building is most affected. The goal is to simultaneously reduce interstory drifts and floor accelerations to limit or avoid damage, not only to the structure but also to its contents, in a cost-effective manner.

Recent years have seen a number of catastrophic structural failures due to severe, impulsive, seismic events. Some researchers (e.g., Hall et al. 1995; Heaton et al. 1995) have raised concerns as to the efficacy of seismic isolation during such events. Based on observations from the January 17, 1994 Northridge earthquake, these researchers suggested that base-isolated buildings are vulnerable to strong impulsive ground motions generated at near-source locations. Moreover, recent revisions to the Uniform Building Code (ICBO 1997) have made the requirements for base-isolation systems more stringent compared to the previous versions (ICBO 1994; Kelly 1999a), potentially rendering the ad-

ditional complexity and cost of base-isolated structures less economically justified (Kelly 1999b). The code-mandated accommodation of larger base displacements and the requirement to consider a stronger Maximum Capable Earthquake has suggested the need for supplemental damping devices (Asher et al. 1996).

The addition of damping, however, may also increase the internal motion of the superstructure as well as increase absolute accelerations, thus defeating many of the gains base isolation is intended to provide (Inaudi and Kelly 1993b; Kelly 1999a,b). To understand the impact of excessive damping, it is important to consider the ever increasing necessity of protecting nonstructural components and highly sensitive equipment such as are found in hospitals, communication centers, and computer facilities. The performance of this equipment can be easily disrupted by moderate acceleration levels and even permanently damaged by higher excitations (Inaudi and Kelly 1993a). Consequently, mitigating damage to the contents of a structure has become a key objective in base isolation design. For example, the 1994 Northridge earthquake "caused extensive destruction of building interiors. Because of the intense shaking and heavy damage to other building elements, sprinkler piping was frequently severed and systems were rendered useless on a much wider scale than has been seen in other earthquakes. Interior partitions, furniture, ceilings, and HVAC and other equipment were destroyed with a thoroughness never before seen on such a scale." (An excerpt from "The January 17, 1994 Northridge, CA Earthquake—An EQE Summary Report," March 1994, by EQE International.) Indeed, some emergency facilities were rendered nonfunctional, not due to superstructure damage, but because they were flooded by water pipes broken due to excessive accelerations within the structure (Hall 1995). The need for hospitals or emergency facilities to be functioning postearthquake is clear. As another example, consider the potential loss of revenue by internet businesses involved in the expanding *e*-commerce market: tremendous financial damage is incurred if their websites and networks crash for a day or two. As a case in point, *USA Today* reported on February 11, 2000 that a single firm, *eBay*, lost $5 million in sales and $4 billion in stock

[1]Research Associate, Laboratorio de Estructuras, Univ. Nacional de Tucumán, Av. Roca 1800, (4000) San Miguel de Tucumán, Tucumán, Argentina. E-mail: jramallo@herrera.unt.edu.ar

[2]Assistant Professor, Dept. of Civil and Environmental Engineering, Univ. of Southern California, Los Angeles, CA 90089-2531 (corresponding author). E-mail: JohnsonE@usc.edu

[3]Linbeck Professor, Dept. of Civil Engineering and Geo. Sci., Univ. of Notre Dame, Notre Dame, IN 46556-0767. E-mail: spencer@nd.edu

value when a hacker shut down its site for only 22 hours. To protect the contents and nonstructural elements in a structure, structural accelerations should be minimized while maintaining acceptable base displacement levels.

Several means of adding damping are available for reducing base drift (base drift demands determine the "seismic gap" required for utilities, connections to adjacent structures or sidewalks, etc.). The three methods most commonly used today passively augment the damping provided by low-damping, natural rubber bearings. Low-damping natural and synthetic rubber bearings typically provide 2–3% of critical damping in the isolation mode. One method of increasing the damping is to use high-damping natural rubber—natural rubber containing extrafine carbon black, oils or resins, and other proprietary fillers (Naeim and Kelly 1999)—that may provide up to 20% isolation mode damping. Another common approach is to install lead plugs in the low-damping laminated rubber bearings to increase energy dissipation through hysteretic damping as the lead plugs shear during large deformation motion. Third, supplemental dampers, such as viscous dampers (both linear and nonlinear, see Taylor and Constantinou 1996) and friction dampers, may be used to augment the damping (Soong and Dargush 1997). Friction pendulum systems (FPSs) are another popular base isolation strategy; though physically different from lead-rubber bearing designs, FPSs may be modeled in a similar manner and exhibit similar behavior. While these passive methods have been used in applications to reduce the deformation demand on the isolation system, the supplemental damping itself tends to drive energy into the higher modes, with corresponding increases in superstructure deformation and acceleration, that may damage the building and its contents (Kelly and Tsai 1985, 1993). Spencer et al. (2000) showed that adding a moderate amount of viscous damping to a low-damping isolation system does decrease responses. However, too much damping can cause accelerations and interstory drifts to go back up (Hall 1999; Spencer et al. 2000), eliminating many of the improvements isolation is intended to provide.

Active and semiactive strategies may be able to provide the reduced base drifts without the increase in superstructure motion seen for passive devices. As reported by Spencer and Sain (1997), a number of analytical studies have focused on the use of active control devices in parallel with a base-isolation system for limiting base drift (e.g., Kelly et al. 1987; Reinhorn et al. 1987; Nagarajaiah et al. 1993; Schmitendorf et al. 1994; Yoshida et al. 1994; Yang et al. 1996). Additionally, Reinhorn and Riley (1994) performed several small-scale experiments to verify the effectiveness of active strategies used in simulation studies. However, active control devices have yet to be fully embraced by practicing engineers, in large part due to the challenges of large power requirements (that may be interrupted during an earthquake), concerns about stability and robustness, and so forth.

Several researchers have investigated the use of smart dampers (also called semiactive or controllable passive dampers) for seismic response mitigation (e.g., Feng and Shinozuka 1990; Nagarajaiah 1994; Makris 1997; Johnson et al. 1999; Kurata et al. 1999; Niwa et al. 1999; Symans and Constantinou 1999; Symans and Kelly 1999; Yoshida et al. 1999). Studies of smart base isolation have used several control design methodologies [such as fuzzy control (e.g., Nagarajaiah 1994; Symans and Kelly 1999), sliding mode control (e.g. Yang et al. 1996), clipped-optimal control (e.g., Johnson et al. 1999; Spencer et al. 2000), etc.] and have examined both bridge and building structures. The first full-scale implementation of smart base isolation was recently constructed at Keio Univ. (Yoshida et al. 1999). The main virtue of these

semiactive controllable systems arises from the combination of the adaptable nature of a fully active control system with the stability characteristic of passive control systems, while maintaining low-power requirements.

The present work investigates the performance of a smart base isolation system and shows that it can reduce base drifts without the accompanying acceleration increases seen with passive strategies. To demonstrate the superior protection provided by smart damping strategies, several historical earthquakes scaled to different magnitudes are used to excite an isolated building structure. A linear, lumped-mass structure model is used as the test bed for this study, first using a two degree-of-freedom (2DOF) model, and then a 6DOF model to examine the effects of higher modes on smart damper performance. The isolation layer characteristics are chosen such that the fundamental mode (the so-called "isolation" mode) has a period of 2.5 s and 2% of critical damping. This configuration is typical of low-damping isolation systems common in engineering practice, is readily attainable using current technology, and follows standard code-based procedures (AASHTO 1991; Naeim and Kelly 1999). Recognizing its worldwide popularity (due mainly to its simplicity and economy), *lead-rubber bearings* (LRBs) are used as a baseline passive isolation system. These self-contained isolation bearings provide both horizontal flexibility and hysteretic damping in a single package, with characteristics determined by pre- and post-yield stiffnesses, and yielding force. After a systematic parameter study using the Bouc-Wen model (Wen 1976) for the LRBs, two "optimal" LRB designs are selected and their limitations/advantages highlighted. Herein, the optimal isolation damping is defined, comparably to Inaudi and Kelly (1993b), as the one which produces a near-minimum peak (absolute) structural acceleration response while providing acceptable small deformations in the isolation system. A *smart damper* system is then designed that is "optimal" over the suite of historical ground motions, achieving significant reductions in the base drift compared to the "optimal" passive damping strategies without increasing the accelerations imparted into the superstructure. Special consideration is given to a rigorous and fair consideration of the performance of smart dampers in comparison with the lead-rubber bearing designs. While passive strategies are shown to effectively isolate the building in many cases, they are suboptimal for a wide range of ground motions. On the other hand, smart dampers are shown to provide a superior base isolation system for a broad class of earthquakes including near-source events as well as for a broad range of input levels. Thus, a smart damper system can protect a structure from extreme earthquakes without sacrificing performance during the more frequent, moderate seismic events.

Model Formulation

Structural System Model

First, the structure is modeled as a single degree-of-freedom (SDOF) system representing the fundamental mode of the five-story building model given by Kelly et al. (1987). In a subsequent section of this paper, a five degree-of-freedom model of the Kelly et al. (1987) building is studied to analyze the effects of higher modes.

When the isolation layer is added, the augmented model is a two degree-of-freedom (2DOF) system. The structural parameters of the SDOF fixed-base and 2DOF isolated structure models are given in Fig. 1. (Two Java applets that demonstrate some of the issues in base isolation design are at http://www.nd.edu/~quake/

java.html.) It has been shown experimentally that the linear behavior of low-damping rubber bearings can extend to shear strains above 100%; moreover, it is possible to manufacture isolators with nearly zero damping and linear shear behavior (Naeim and Kelly 1999). Therefore, the isolation layer is modeled as a linear Kelvin-Voigt element—i.e., linear stiffness and viscous damping—and gives a fundamental mode with a 2.5 s period and 2% of critical (viscous) damping. (The forces generated by the multiple isolation bearings typical in a low-damping isolation system are modeled here by their combined stiffness and damping characteristics.) This low-damping, long-period, isolation system is a typical design and falls in the "*Class (ii): lightly damped, linear isolation system*" category of Skinner et al. (1993).

Assuming the structural motion is sufficiently moderate that nonlinear effects may be neglected, and denoting the base and structure displacements relative to the ground by $\mathbf{x} = [x_b \ x_s]^T$, the equations of motion of the base-isolated system may be expressed as

$$\mathbf{M}\ddot{\mathbf{x}} + \mathbf{C}\dot{\mathbf{x}} + \mathbf{K}\mathbf{x} = \mathbf{\Lambda}f - \mathbf{M}\mathbf{1}\ddot{x}_g \qquad (1)$$

where f = supplemental force exerted by the smart damper or the LRB lead plug; $\mathbf{\Lambda} = [1 \ 0]^T$ gives the position of the supplemental damper force; $\mathbf{1}$ = vector whose elements are all unity; $\ddot{x}_g$ = absolute ground acceleration; and the mass, damping, and stiffness matrices are, respectively,

$$\mathbf{M} = \begin{bmatrix} m_b & 0 \\ 0 & m_s \end{bmatrix}, \quad \mathbf{C} = \begin{bmatrix} c_b + c_s & -c_s \\ -c_s & c_s \end{bmatrix}, \quad \mathbf{K} = \begin{bmatrix} k_b + k_s & -k_s \\ -k_s & k_s \end{bmatrix} \qquad (2)$$

Defining states $\mathbf{q} = [\mathbf{x}^T \ \dot{\mathbf{x}}^T]^T$; outputs to be regulated $\mathbf{z} = [x_b \ (x_s - x_b) \ \ddot{x}_b^a \ \ddot{x}_s^a]^T$ including interstory drifts and absolute floor accelerations; and sensors $\mathbf{y} = [x_b \ \ddot{x}_b^a \ \ddot{x}_s^a \ \ddot{x}_g]^T + \mathbf{v}$ measuring base drift, absolute floor accelerations, and absolute ground acceleration ($\mathbf{v}$ is a vector of sensor noises modeled as independent, Gaussian white-noise processes), the state-space form of the equations of motion is given by

$$\dot{\mathbf{q}} = \mathbf{A}\mathbf{q} + \mathbf{B}f + \mathbf{E}\ddot{x}_g$$
$$\mathbf{z} = \mathbf{C}_z\mathbf{q} + \mathbf{D}_z f$$
$$\mathbf{y} = \mathbf{C}_y\mathbf{q} + \mathbf{D}_y f + \mathbf{F}_y\ddot{x}_g + \mathbf{v}$$

$$\mathbf{A} = \begin{bmatrix} \mathbf{0} & \mathbf{I} \\ -\mathbf{M}^{-1}\mathbf{K} & -\mathbf{M}^{-1}\mathbf{C} \end{bmatrix} \quad \mathbf{B} = \begin{bmatrix} \mathbf{0} \\ \mathbf{M}^{-1}\mathbf{\Lambda} \end{bmatrix} \quad \mathbf{E} = \begin{bmatrix} \mathbf{0} \\ -\mathbf{1} \end{bmatrix}$$

$$\mathbf{C}_z = \begin{bmatrix} \mathbf{\Delta} & \mathbf{0} \\ -\mathbf{M}^{-1}\mathbf{K} & -\mathbf{M}^{-1}\mathbf{C} \end{bmatrix} \quad \mathbf{D}_z = \begin{bmatrix} \mathbf{0} \\ \mathbf{M}^{-1}\mathbf{\Lambda} \end{bmatrix} \quad \mathbf{\Delta} = \begin{bmatrix} 1 & 0 \\ -1 & 1 \end{bmatrix}$$

$$\mathbf{C}_y = \begin{bmatrix} 1 & 0 & 0 & 0 \\ -\mathbf{M}^{-1}\mathbf{K} & -\mathbf{M}^{-1}\mathbf{C} \\ 0 & 0 & 0 & 0 \end{bmatrix} \quad \mathbf{D}_y = \begin{bmatrix} 0 \\ \mathbf{M}^{-1}\mathbf{\Lambda} \\ 0 \end{bmatrix} \quad \mathbf{F}_y = \begin{bmatrix} 0 \\ 0 \\ 1 \end{bmatrix}$$

where $\mathbf{\Delta}$ = matrix giving interstory drifts.

$\qquad (3)$

Damping Systems

Lead-rubber bearings are considered as the baseline against which the smart damping strategies are compared. The modeling approaches for these two systems are described as follows:

- *Lead-rubber bearing* (LRB): the horizontal force required to induce the LRB into its post-yield phase can be expressed as the sum of three forces acting in parallel

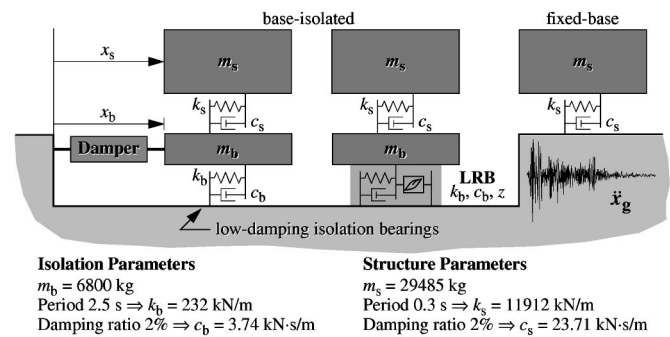$$f_{\text{LRB}} = Q_{\text{Pb}} + k_b x_b + c_b \dot{x}_b \qquad (4)$$

Fig. 1. Two degree-of-freedom (2DOF) models

where $Q_{\text{Pb}} = (1 - K_{\text{yield}}/K_{\text{initial}}) \cdot Q_y$ = yield force of the lead plug; Q_y = yield force from both the lead plug and the rubber stiffness; k_b and c_b = horizontal stiffness and viscous damping coefficient of the rubber composite of the bearing; and x_b and $\dot{x}_b$ = relative displacement and velocity across the bearing. The damping component of f_{LRB} is mainly generated by the hysteretic behavior of the lead plug inserted into the rubber bearing, although the (small) viscous damping component $c_b\dot{x}_b$ may be attributed to the damping characteristics of the rubber. The hysteretic behavior of the LRB (Fig. 2) is often treated as a bilinear solid (Kikuchi and Aiken 1997) with initial shear stiffness K_{initial}, and postyield shear stiffness $K_{\text{yield}} = k_b$ (Skinner et al. 1993). This bilinear model, however, causes overestimation of the acceleration levels in base-isolated structures. In contrast, a Bouc-Wen model (Wen 1976) gives results more consistent with experimental data (Nagarajaiah and Xiaohong 2000). Consequently, the LRB is modeled herein using the Bouc-Wen model, which includes an evolutionary variable z to account for the hysteretic component of the force $Q_{\text{hyst}} = zQ_{\text{Pb}}$. The differential equation governing the evolutionary variable z is given by

$$\dot{z} = -\gamma|\dot{x}_b|z|z|^{n-1} - \beta\dot{x}_b|z|^n + A\dot{x}_b \qquad (5)$$

where γ, β, A, and n = shape parameters of the hysteresis loop which herein are considered time invariant. To model the initial stiffness properly, it is required that $A = K_{\text{initial}}/Q_y$. For unloading to follow the preyield stiffness, $\gamma = \beta$. For the postyield purely plastic behavior of the lead plug [i.e., Eq. (4)], the evolutionary variable z will approach unity and $Q_{\text{hyst}} = Q_{\text{Pb}}$ when $A = \gamma + \beta$. Finally, the parameter n, which governs the sharpness of the transition from initial to final stiffness, is chosen to be 1 (Spencer 1986). Thus, $n = 1$ and $A = 2\gamma = 2\beta$
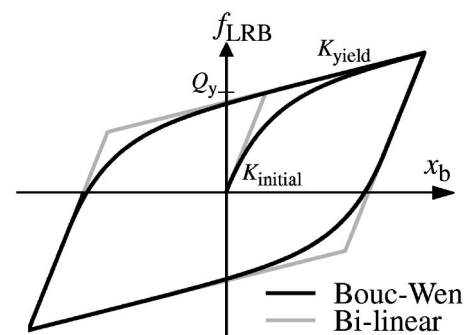

Fig. 2. Lead-rubber bearing (LRB) hysteretic models

$=K_{\text{initial}}/Q_y$.

The postyield stiffness k_b, generated by the stiffness of the rubber, is fixed so as to give a 2.5 s fundamental postyield period (Skinner et al. 1993). The preyield to postyield stiffness ratio and the LRB yield force Q_y are left to be design parameters; two sets of values will be studied herein that give good performance in moderate and severe ground motions, respectively. The viscous damping c_b from the rubber is assumed to give 2% viscous damping in the absence of the lead plug.

- *Smart (semiactive) damper*: a controllable damper (e.g., controllable fluid damper, variable orifice damper, etc.; see Spencer and Sain 1997; Symans and Constantinou 1999) that may only exert dissipative forces; i.e., $f_{\text{SA}}\dot{x}_b \leq 0$ where f_{SA} is the force applied by the damper and $\dot{x}_b$ is the velocity across the damper. For this study, the device is assumed ideal; i.e., it can generate the desired (dissipative) forces with no delay and with no actuator dynamics.

The rubber isolation in these two systems is identical. The difference between the two systems is that one has a lead plug to give the supplemental damping, whereas the other has a smart damper instead. To make for a fair comparison, the peak force of the smart damper is limited. The lead-rubber bearings are subsequently shown to perform well for severe ground motions with a yield force about 15% of the total weight of the building—consistent with the recommendations in the literature (Skinner et al. 1993; Wang and Liu 1994; Park and Otsuka 1999). Thus, for fair comparison, the smart damper force will be limited to 53.39 kN (15% of the total weight of the building). This limit in the damping force is enforced using a saturation criteria to clip the damper force to be within the limits (see, for instance, Fig. 4).

Ground Excitation

The isolated structures considered herein are excited by a suite of ground motions that are intended to encompass both moderate events

- *El Centro*—north-south component of the 1940 Imperial Valley, Calif. earthquake (magnitude 7.1) recorded at Imperial Valley Irrigation District substation in El Centro, Calif.;
- *Hachinohe*—north-south component of the 1968 Takochi-oki (Hachinohe) earthquake (magnitude 7.9) signal recorded at Hachinohe City, Japan;

and severe events

- *Kobe*—north-south component of the 1995 Hyogo-ken Nanbu (Kobe) earthquake (magnitude 7.2) recorded at the Kobe Japanese Meteorological Agency (JMA), Kobe, Japan;
- *Northridge*—north-south component of the 1994 Northridge earthquake (magnitude 6.8) recorded at the Sylmar County Hospital parking lot in Sylmar, Calif.

Additionally, the earthquakes are scaled to several magnitudes to better understand the effectiveness of the isolation strategies for different earthquake strengths. The moderate records are scaled in the range from 0.5 to 2.0 times the historical record, and the severe ones from 0.5 to 1.5. Although magnifying the severe earthquakes might seem unnecessary, the results using 1.5 times historical records are included to show the behavior of different damping devices under extreme, but conceivable, events.

Smart Damping Strategies

Several studies have focused on the use of hybrid control schemes composed of damping devices in parallel with a base isolation
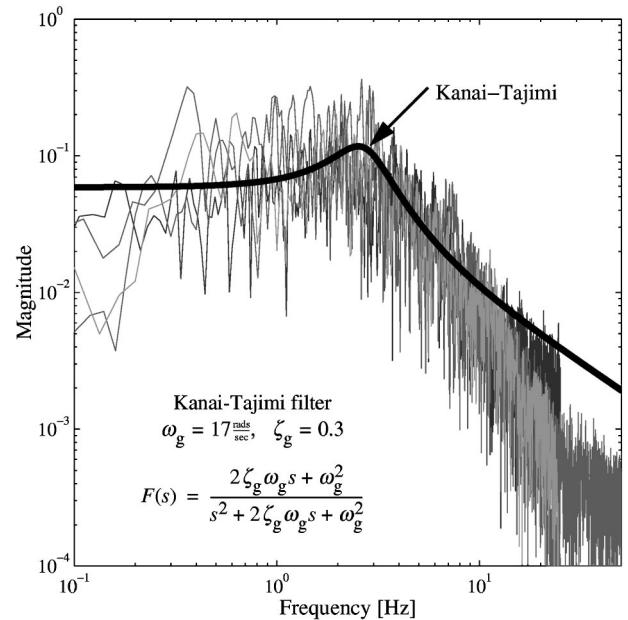

Fig. 3. Frequency content of design earthquakes and Kanai-Tajimi shaping filter

system (Spencer and Sain 1997). A *clipped-optimal* control strategy, shown to perform well in previous works involving smart dampers (e.g., Dyke et al. 1996a,b; Johnson et al. 1999, 2003; Spencer et al. 2000), is implemented in this study. The strategy is to assume an ''ideal'' actively controlled device, design an appropriate *primary* controller for this active device, and then use a *secondary* controller which clips the optimal control force so it is dissipative in a manner consistent with the physical nature of the device. [In an experimental implementation, the dissipation requirement is enforced implicitly by the device; a secondary controller is still necessary to make the actual force track the desired force commanded by the primary controller (Dyke et al. 1996a,b)].

To better inform the primary controller about the frequency content of the ground motion, a Kanai-Tajimi (Soong and Grigoriu 1993) shaping filter is incorporated into the model of the system. Fig. 3 shows the magnitude of this filter as a function of frequency, as well as the frequency content of magnitude-scaled versions of the four historical design earthquakes. An H_2/LQG (linear quadratic Gaussian) controller is then designed for the combined filter/structure model, such as shown in Fig. 4(a). Assuming independence of the ground excitation and measurement noises, the interstory drifts and absolute floor accelerations are weighted using the cost function

$$J = \lim_{\tau \to \infty} \frac{1}{\tau} E\left[\int_0^\tau (\mathbf{z}^T\mathbf{Q}\mathbf{z} + Rf_A^2)dt \right] \qquad (6)$$

with control weight $R = (22 \text{ kN})^{-2}$ and a diagonal evaluation weighting matrix:

$$\mathbf{Q} = \begin{bmatrix} q'_{\text{drifts}}\mathbf{I} & \mathbf{0} \\ \mathbf{0} & q'_{\text{accels}}\mathbf{I} \end{bmatrix} \qquad (7)$$

where $q'_{\text{drifts}} = 144 \text{ m}^{-2} q_{\text{drifts}}$ and $q'_{\text{accels}} = (\text{m/s}^2)^{-2} q_{\text{accels}} =$ scalar only 2 columns drift and acceleration weights, and $\mathbf{I} = 2 \times 2$ identity matrix. By adjusting the nondimensional values q_{drifts} and q_{accels}, various levels of control performance are achieved. The
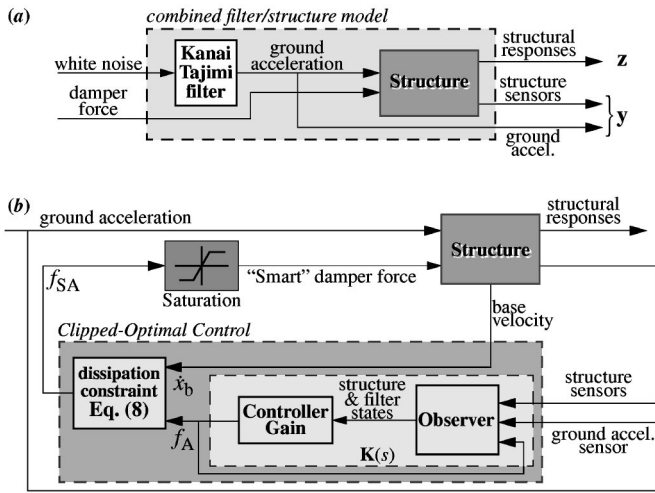
Fig. 4. (a) Combined filter/structure model for which primary controller is designed. (b) Smart damper control strategy using clipped-optimal controller.
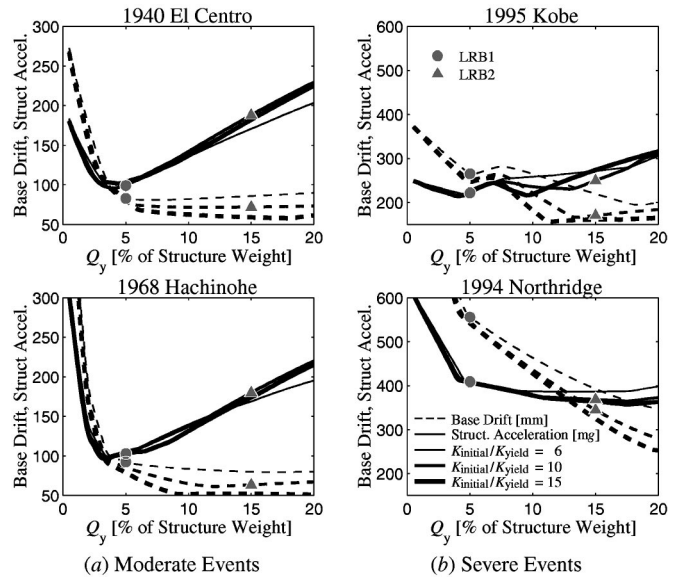

Fig. 5. Peak responses of lead-rubber bearing-isolated building under (a) moderate and (b) severe seismic actions

H_2/LQG primary controller is then designed using the Control Toolbox in MATLAB®, resulting in a dynamic compensator $\mathbf{K}(s)$ of order six (the sum of the orders of the structure and the shaping filter). The sensor noises $\mathbf{v}$ are assumed uncorrelated with standard deviations $[0.01/12\ s^2, 0.01, 0.01, 0.035]$ times that of the ground acceleration disturbance.

The secondary controller is given by

$$f_{SA} = \begin{cases} f_A & \text{if } f_A \dot{x}_b < 0 \\ 0 & \text{otherwise} \end{cases} \tag{8}$$

where f_A = "desired" force that would be applied if using an active device and $\dot{x}_b$ = velocity across the damper. Because the smart damper is an intrinsically nonlinear *energy dissipation* device and cannot add mechanical energy to the structural system, finding high-performance clipped-optimal controllers generally requires a numerical search over the parameters in the weighting matrix $\mathbf{Q}$. This is the method used here. Note that effective controllers for smart damping devices typically have *primary* controllers (here, the H_2/LQG design) that command a dissipative "desired" force f_A during the majority of the seismic event. (Otherwise, the force would be set to zero a majority of the time.) The clipped-optimal controller is shown in Fig. 4(b). Note that a saturation block is used to limit the peak forces as discussed previously.

There is one unusual aspect to this control design. The force fed back to an observer is usually the force actually applied to the system (e.g., Dyke et al. 1996a,b; Johnson et al. 2003). Here, that would be f_{SA} or a saturated version thereof. However, it was found that feeding back the "desired" force f_A gave superior performance. The reason, perhaps, is due to the dissipation constraint enforced by Eq. (8), which causes sudden on/off switching of the smart damper force that induces transient step responses in the observer, thereby causing yet larger swings in both the force commanded and actually applied. These swings were seen to cause larger accelerations, particularly at the base, than if the "desired" force is fed back. Thus, since good closed-loop performance is the objective, the "desired" force is fed back, as in Fig. 4(b), for the results shown herein.

Designing the "Optimal" Passive Isolation System

Lead-Rubber Bearings

In the design of lead-rubber bearings for this study, the influence of two parameters is considered, namely, the total yield force Q_y [expressed as a fraction of the total building (base + superstructure) weight] and the preyield to postyield stiffness ratio $K_{initial}/K_{yield}$. The postyield stiffness is held fixed at $K_{yield} = k_b = 232$ kN/m to obtain a fundamental period of 2.5 s once the lead plug has yielded. While the optimal value of the yield force Q_y will depend on the flexibility of the superstructure as well as the excitation (Inaudi and Kelly 1993a,b), for design earthquakes having the severity and "character" of the El Centro earthquake, Skinner et al. (1993) suggest typical values of the yield force Q_y on the order of 5% of the total weight of the building.

Fig. 5 shows peak base drifts and peak absolute accelerations (maximum of base and structural accelerations over time) of the 2DOF model as a function of the yield force Q_y for several values of the stiffness ratio $K_{initial}/K_{yield}$. The plots corresponding to moderate events (left-hand side) show close agreement with the design yield force given by Skinner and his coworkers, particularly regarding the reduction of base drift. Note that the peak absolute accelerations do decrease with increasing (but small) Q_y—but only up to $Q_y \approx 4\%$ of building weight. After that, interstory drifts (not shown) and accelerations increase significantly. Therefore, a lead-rubber bearing, designed for the El Centro and Hachinohe earthquakes (the moderate earthquakes), with $Q_y = 5\%$ of the building weight and $K_{initial}/K_{yield} = 6$, is designated LRB1. Higher-stiffness ratios also give similar results, but the ratio of six is more typical of that used in practice (Skinner et al. 1993). This design Q_y follows the results of Park and Otsuka (1999), who compare different methods to determine an "Optimal Yield Ratio," giving Q_y from 4.3 to 5.0% of structure mass for moderate earthquakes [peak ground acceleration (PGA) of $0.35g$]—this substantiates Skinner's aforementioned suggestion and the design here. The responses with this LRB1 design are shown as circles on the graphs in Fig. 5. The LRB1 design is then used as the basis against which the other supplemental damping devices will be compared.

To achieve similar results for scaled versions of the El Centro earthquake, the yield force must be scaled by the same factor (Skinner et al. 1993). Moreover, since the set of earthquakes includes severe events (Kobe and Northridge), higher-yield strengths may be necessary. And indeed this is the case as is clearly depicted in Fig. 5 (right-hand side): in order to obtain significant reductions in base drifts and moderate accelerations for the severe ground motions, the yield force must be 13–17% of the building weight, with a suitable stiffness ratio around ten. Indeed, Park and Otsuka (1999) find Q_y in the range from 14 to 18% to be best for more severe ground motions (PGA of 1.225g). Hence, a second design, called LRB2, with yield force Q_y =15% of the building weight and with stiffness ratio $K_{initial}/K_{yield}$= 10, is also studied. The responses of the LRB2 design are denoted by triangles in Fig. 5. It should be emphasized that LRB designs for severe events, such as the LRB2 design, are not common in practice; however, the concerns about large base drifts in strong near-fault ground motion (e.g., Hall et al. 1995; Heaton et al. 1995) have prompted researchers to consider such designs.

In the remainder of this study, the performance of the high-damping lead-rubber bearing LRB2 design and a smart damper strategy will be compared to the performance of the low-damping lead-rubber bearing LRB1 design. The selection of LRB1 as the basis for comparison is supported by the fact that it is the optimal LRB system for the (unscaled) El Centro earthquake.

Smart Controllable Damper

A thorough parameter study is performed to determine appropriate H_2/LQG weighting matrices for efficient controllable damping strategies. A family of controllers that decreases base drift and absolute accelerations (compared to the LRB1) is obtained for a controllable smart damper. As mentioned previously, the maximum damper force is limited to 15% of the total weight of the building using a saturation element (see Fig. 4).

Preliminary parameter studies showed that some output weights in the ranges

$$q_{drift} \in [0.05, 10.0] \quad q_{acccls} \in [1.0, 10.0] \quad (9)$$

made improvements in both peak base drift and peak accelerations compared to the LRB1 baseline. The hatched areas in Fig. 6 denote the regions where, using a smart damper, the peak absolute accelerations for both base and superstructure are decreased for all four (unscaled) historical earthquakes compared to the LRB1 design. The contour lines depict minimum improvements (i.e., reductions) in base drift. Note that these are "worst-case" improvements in the suite of four historical earthquakes; thus, substantial improvements (i.e., much better than the worst-case shown in Fig. 6) are possible with smart dampers for some of the ground motions (shown in the next section).

To investigate the gains that may be achieved with smart damping systems, one particular control design was chosen, with q_{drifts}=0.5974, q_{accels}=2.6701; this point is shown in Fig. 6 as a small circle. Using this particular control design, the 2DOF isolated building was simulated and peak responses computed for base drift and acceleration, structural drift and acceleration, damper force, and base shear.

Two Degree-of-Freedom Results

Table 1 shows the responses of the structural system with the LRB1 baseline design (i.e., the LRB with Q_y=5% of the build-
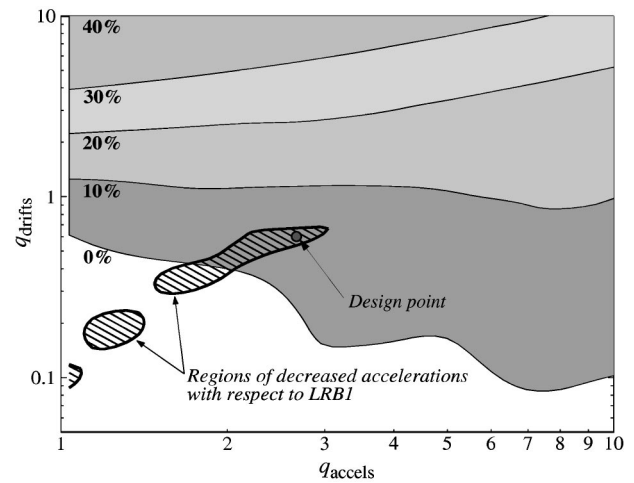

Fig. 6. Regions of smart damper improvement compared to the LRB1 baseline

ing weight and $K_{initial}/K_{yield}$=6) to various earthquakes. Table 2 reports the percent response improvement ($+$) or detriment ($-$) compared to the LRB1 system for four cases: (1) the smart isolation system; (2) LRB2 (high-damping passive lead-rubber bearing); (3) the rubber alone with no supplemental damping (i.e., 2% damping from the rubber in the isolation layer); and (4) the fixed base structure. The peak base drift, structural acceleration, and supplemental force (lead plug or smart damper) relative to LRB1 are shown in Fig. 7 for smart damper isolation and LRB2.

From Table 2 it can be seen that the LRB2 system, due to its higher-yield level, is capable of substantial reductions in the peak base drift. For severe seismic events, reductions in base drift reach a maximum of about 50%. Note that this improvement of the LRB2 system over the LRB1 system diminishes in the case of the Northridge earthquake as the earthquake scale increases. A similar trend is found for the Kobe earthquake when the scale is increased to 1.5, while for the moderate earthquakes peak base drifts are reduced as the scale factor increases, from 5% to about 53%. Not surprisingly, however, these reductions in base drift come at the price of increased accelerations, interstory drifts, and base shears. Peak accelerations in the LRB2 system were increased for 12 of the 14 ground motions considered, sometimes substantially increased, while only marginally decreased in the other two ground motions. Moreover, for the reduced-scale moderate earthquakes (i.e., those that are likely to occur more frequently), the accelerations increased up to 2.37 times that found for the LRB1 system. Structural drifts and base shears follow a pattern similar to structural acceleration.

In contrast, the smart damping system performs well over the entire suite of earthquakes considered. The reductions in peak base drift are comparable to those of the LRB2 isolation system—both giving as much as nearly 55% decreased base drift compared to LRB1 isolation. The smart damper achieves decreases in peak accelerations, structural drifts, and base shears for most cases, as much as 44% in some cases. In contrast, the LRB2 design *increases* these responses, often by significant amounts (over double that of the LRB1 response for small earthquakes). In contrast to the LRB2 system, the decrease in the base drift during the large earthquakes afforded by a smart damper does not come at the expense of larger accelerations, interstory drifts, and base shears.

Table 1. Two Degree-of-Freedom Peak Drifts, Absolute Accelerations and Forces for LRB1

Earthquake	PGA (g)	Drift (mm)		Acceleration (mg)		Base force (kN)	
		Base	Structure	Base	Structure	Lead	Shear
0.5×El Centro	0.1747	41.0	1.64	68.7	67.7	14.38	23.86
1.0×El Centro	0.3495	82.9	2.41	109.1	99.3	14.83	34.06
1.5×El Centro	0.5242	167.7	3.69	155.8	152.0	14.83	53.84
2.0×El Centro	0.6990	300.6	5.82	234.7	239.5	14.83	84.74
0.5×Hachinohe	0.1147	41.9	1.70	72.8	69.9	14.63	24.37
1.0×Hachinohe	0.2294	92.6	2.50	111.6	103.0	14.83	36.38
1.5×Hachinohe	0.3440	168.3	3.70	153.1	152.4	14.83	53.94
2.0×Hachinohe	0.4587	312.1	5.99	240.2	246.6	14.83	87.34
0.5×Kobe	0.4168	132.4	3.14	124.9	129.2	14.83	45.67
1.0×Kobe	0.8337	265.3	5.38	233.3	221.7	14.83	76.48
1.5×Kobe	1.2505	454.0	8.27	351.6	340.7	14.83	120.36
0.5×Northridge	0.4214	231.7	4.70	198.3	193.6	14.83	68.65
1.0×Northridge	0.8428	556.0	9.93	410.9	409.0	14.83	143.99
1.5×Northridge	1.2642	1013.9	17.17	722.1	707.3	14.83	250.29

With regard to the peak forces, the LRB lead plugs attained, in most cases, their yield forces (for LRB1, $F_{yield} = Q_{Pb} = 14.83$ kN; for LRB2, $F_{yield} = Q_{Pb} = 48.05$ kN). The smart damper uses rather smaller forces for small ground motions but hits the saturation limit for strong ground motions (historical or larger Northridge or Kobe motions). Note that the peak force exerted by the smart damper is well within the range of current technology. The peak force here was 53.39 kN for a scaled building—for a similar full-scale structure, the forces can be generated with parallel configurations of dampers based on current technology. For example, a prototype 200 kN semiactive magnetorheological fluid damper has been developed at the Univ. of Notre Dame (Spencer and Sain 1997). Typical force-displacement loops are shown for two historical earthquakes in Fig. 8. Two observations are important here. First, the smart isolation uses force levels similar to LRB1 in the El Centro earthquake, but more like LRB2 for the stronger Kobe earthquake, demonstrating the adaptive nature of the smart isolation. Second, the smart isolation has rounded corners on the loops, giving more moderate acceleration levels than the LRB designs.

Influence of Higher Modes

To study the influence of higher modes on the performance of the base isolation systems, the six degree-of-freedom isolated building model depicted in Fig. 9 is used. The parameters of the superstructure are the same used in Kelly et al. (1987), while the properties of the isolation layer (i.e., k_b and c_b) are the same as in the 2DOF system described previously. The structural parameters, listed in Table 3, give the same 2.5 s period, $\zeta = 2\%$ isolation mode, and the same fixed-base fundamental 0.3 s, $\zeta = 2\%$ mode as in the 2DOF problem.

This 6DOF structural model is numerically simulated for the same isolation systems as studied for the 2DOF model. Again, one LRB design (discussed further in the next paragraph) will be used as a baseline. The other strategies are: (1) the smart isolation system; (2) a second LRB design (high-damping passive lead-rubber bearing); (3) the rubber alone with no supplemental damping (i.e., 2% damping from the rubber in the isolation layer); and (4) the fixed base structure. The same suite of unscaled historical earthquakes are used to determine "optimal" designs for each isolation method. Those designs are then simulated for unscaled and scaled ground motions.

Lead-Rubber Bearings

The optimal systems selected for the 2DOF structure (i.e., LRB1 with yield force $Q_y = 5\%$ of the weight of the building and preyield to postyield stiffness ratio $K_{initial}/K_{yield} = 6$, and LRB2 with $Q_y = 15\%$ and $K_{initial}/K_{yield} = 10$) are also near-optimal lead-rubber bearing designs for the 6DOF building model. Fig. 10 depicts the peak responses of the 6DOF structure—peak base drift and peak absolute acceleration (maximum over all levels, m_b to m_5)—as a function of the yield force Q_y (expressed as a percent of the building's total weight) and for three different stiffness ratios $K_{initial}/K_{yield} = 6, 10, 15$. For moderate ground motions (left-hand-side plots), the parameters selected for LRB1 are still near optimal. (Choosing a $Q_y \cong 4\%$ would slightly improve peak accelerations, but with some increase in base drift.) For severe ground motions (right-hand-side plots), a yield force level of 15% is again nearly optimal, particularly for the Northridge record. A stiffness ratio of six would result in smaller accelerations for Kobe but with larger drifts. However, for consistency with the 2DOF analysis—and in accordance with actual design recommendations (Kelly 1997; Naeim and Kelly 1999)—the stiffness ratio value of $K_{initial}/K_{yield} = 10$ is retained here also.

Smart Controllable Damper

For smart damping of the 2DOF system, four sensors were used: base drift and absolute accelerations of the base, the structure, and the ground. The superstructure in the 2DOF model is a single mass. Now, the 6DOF model has five distinct structural accelerations that may be measured. To allow for fair side-by-side comparison, the number (and type) of sensors will be held constant.

If the controller designed for the 2DOF model is to be used directly for the 6DOF system, the only question is which structure mass should be instrumented. Analyzing the frequency response of the superstructure of the 2DOF model and comparing them with the frequency responses of the five superstructure masses of the 6DOF model, it can be shown that the best corresponding superstructure acceleration is the roof acceleration (mass m_5). Now, it is possible to use the six-state controller designed for the

Table 2. Percent Improvement (i.e., Reduction) Compared to LRB1 for Two Degree-of-Freedom Model (Positive Numbers are Better)

Earthquake	PGA (g)	Base Drift			Structural Drift				Base Acceleration			Structural Acceleration				Supplemental Force		Base Shear			
		Smart	LRB2	Rubber	Smart	LRB2	Rubber	Fixed	Smart	LRB2	None	Smart	LRB2	Rubber	Fixed	Smart	LRB2	Smart	LRB2	Rubber	Fixed
0.5×El Centro	0.1747	3.4	5.1	−285.6	33.1	−117.8	−53.1	−673.0	20.4	−137.7	−49.7	33.0	−117.8	−53.1	−673.4	18.6	−193.1	35.6	−114.6	−54.0	−534.5
1.0×El Centro	0.3495	4.3	13.1	−281.9	8.7	−89.6	−108.8	−954.2	−0.3	−97.8	−88.6	8.7	−89.6	−108.8	−954.7	−57.9	−218.1	9.7	−87.7	−115.8	−789.0
1.5×El Centro	0.5242	29.0	35.9	−183.2	10.6	−40.4	−104.5	−932.6	−5.3	−79.5	−98.0	10.5	−40.4	−104.5	−933.2	−136.8	−222.9	14.3	−35.4	−104.8	−743.7
2.0×El Centro	0.6990	47.2	51.7	−110.6	24.3	−0.6	−73.0	−773.7	6.8	−44.5	−75.3	24.3	−0.6	−73.0	−774.2	−215.8	−223.8	27.4	3.5	−73.5	−614.7
0.5×Hachinohe	0.1147	15.7	15.3	−573.5	50.3	−100.8	−163.9	−504.0	42.2	−91.4	−150.0	50.3	−100.8	−163.9	−504.4	15.9	−181.8	52.3	−103.0	−168.7	−401.8
1.0×Hachinohe	0.2294	23.8	31.4	−508.9	32.5	−74.8	−258.5	−720.5	24.6	−70.6	−226.3	32.4	−74.8	−258.4	−721.0	−65.9	−219.4	36.0	−70.9	−260.0	−572.3
1.5×Hachinohe	0.3440	37.1	42.0	−402.7	31.5	−35.2	−263.3	−731.6	17.5	−51.7	−256.8	31.5	−35.2	−263.3	−732.2	−148.9	−223.7	35.3	−31.1	−264.2	−580.1
2.0×Hachinohe	0.4587	54.8	52.8	−261.5	43.6	3.1	−199.4	−585.3	29.9	−13.8	−203.3	43.6	3.1	−199.4	−585.8	−231.8	−224.0	46.7	5.7	−199.9	−460.0
0.5×Kobe	0.4168	39.3	24.3	−45.3	26.0	−58.7	2.2	−834.4	31.9	−98.1	1.1	26.0	−58.7	2.2	−834.9	−98.1	−223.6	28.8	−56.3	2.0	−665.2
1.0×Kobe	0.8337	39.4	35.7	−45.1	13.7	−12.6	−14.1	−989.3	6.1	−65.3	−5.9	13.7	−12.6	−14.0	−989.7	−260.0	−224.0	14.9	−15.0	−17.0	−813.7
1.5×Kobe	1.2505	45.1	26.8	−27.2	22.9	−3.9	−11.3	−963.2	−4.2	−42.5	−5.4	22.9	−3.9	−11.3	−963.8	−260.0	−224.0	26.8	−4.3	−11.5	−771.0
0.5×Northridge	0.4214	41.6	50.8	−109.7	23.6	−8.7	−64.4	−729.2	26.2	−12.5	−57.1	23.6	−8.7	−64.4	−729.7	−170.3	−223.9	26.4	−8.3	−64.3	−576.8
1.0×Northridge	0.8428	42.8	38.0	−74.7	25.5	9.9	−55.6	−685.0	17.0	4.0	−51.6	25.5	9.9	−55.6	−685.5	−260.0	−224.0	28.6	11.0	−56.7	−545.4
1.5×Northridge	1.2642	41.3	35.5	−43.7	31.0	20.2	−35.0	−581.0	16.1	17.6	−29.4	31.0	20.2	−35.0	−581.4	−260.0	−224.0	33.8	20.1	−35.2	−456.9
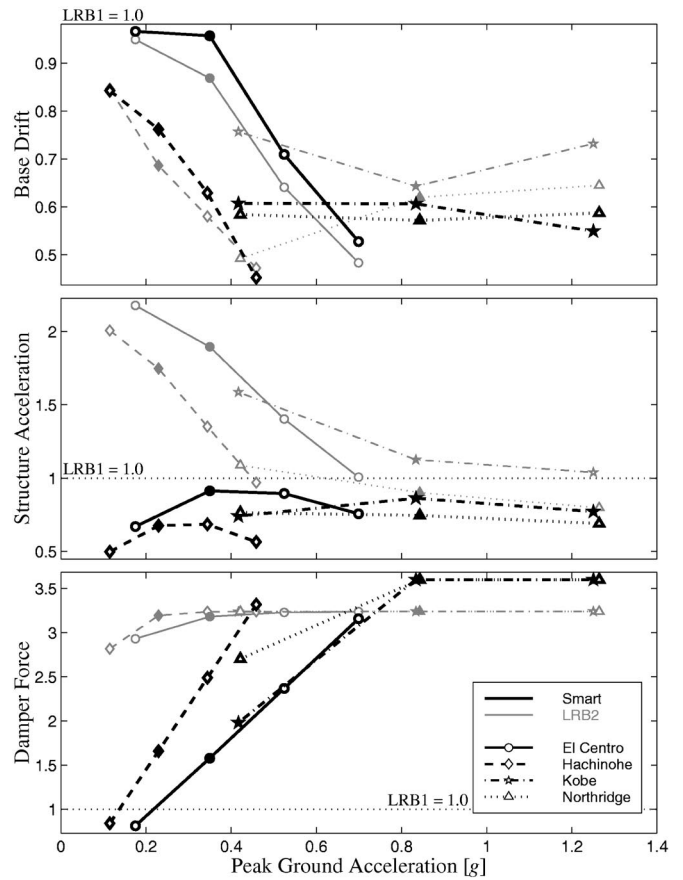
Fig. 7. Peak base drift, structural acceleration, and damper force for the two degree-of-freedom model relative to LRB1. Filled markers denote responses due to unscaled historical earthquakes.

earthquakes are used to determine "optimal" designs for each $=0.5974$ and $q_{accels}=2.6701$] in the 6DOF structure as it requires the same number and types of inputs. The resulting smart damper strategy gives good, but not quite optimal, results (not shown here for the sake of brevity).

Taking a further step to capitalize on a higher-order controller based on the 6DOF model, the same procedure described for the 2DOF system is followed to design a controller with the weighting matrix

$$\mathbf{Q}=\mathrm{diag}([\, q'_{\mathrm{drifts}}[1\ 0\ 0\ 0\ 0\ 0] \quad q'_{\mathrm{accels}}[1\ 0\ 0\ 0\ 0\ 1]\,])$$
(10)

(which weights the base drift, the absolute base acceleration, and the absolute roof acceleration) and the same sensor measurements as before (i.e., base drift, base, roof (mass m_5), and ground accelerations). A new region of the weighting space q_{drifts} versus q_{accels} was found where the smart damper reduces base drift compared to LRB1 without increasing accelerations. Fig. 11 (a close relative of Fig. 6) shows the region where the smart damper can provide reductions in base displacement (contour lines) while not increasing the floor accelerations (hatched region) for the suite of unscaled historical earthquakes. From this optimal (hatched) zone, a particular point was chosen ($q_{\mathrm{drifts}}=31.1$ and $q_{\mathrm{accels}}=99.3$) and the 6DOF system simulated.

Six Degree-of-Freedom Results

Table 4 shows the results in terms of peak interstory drifts and absolute accelerations at different floor levels, as well as peak
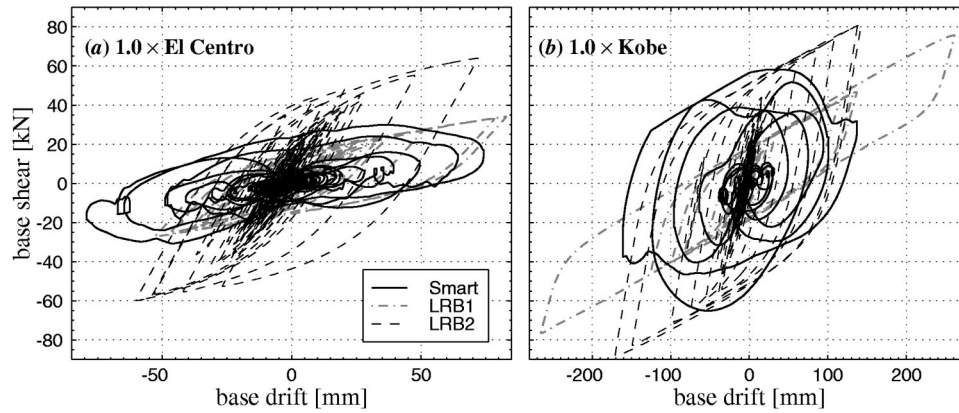
Fig. 8. Force-displacement loops with LRB1, LRB2, and smart isolation of two degree-of-freedom system for two historical earthquakes
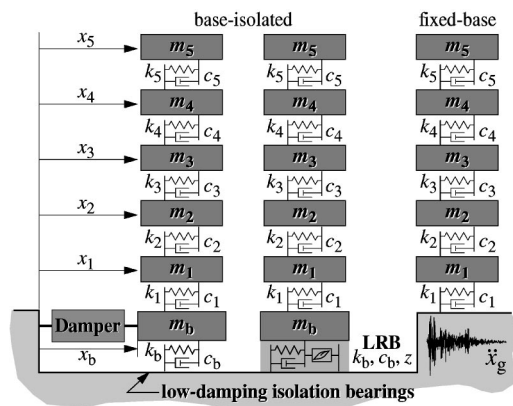

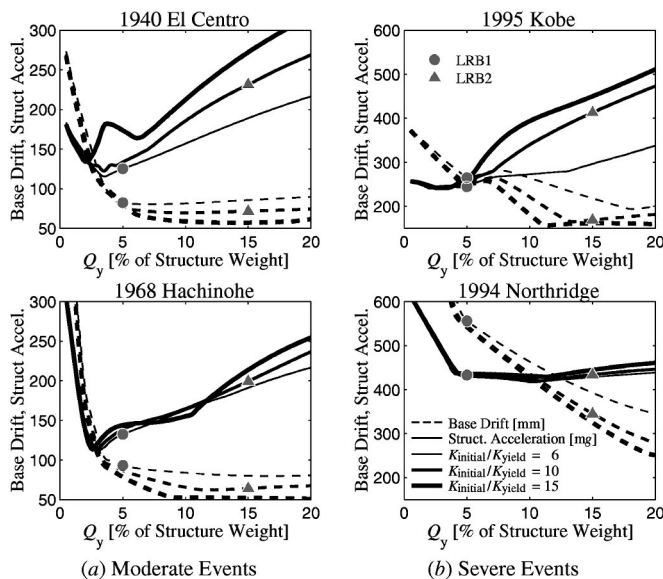**Fig. 9.** Multi-degree-of-freedom (MDOF) models

Fig. 10. Peak seismic responses of LRB-isolated building (six degree-of-freedom model)

damper forces and base shears, for the 6DOF base-isolated building model using the LRB1 system and excited by the unscaled and scaled historical earthquakes. Percent improvements (positive values) and detriments (negative values) provided by the fixed-base structure and by the three isolation strategies compared to LRB1 are reported in Table 5. The peak base drift, structural acceleration, and damper force relative to LRB1 are shown in Fig. 12 for smart dampers and LRB2. To effectively analyze this data, two different viewpoints are used.

First, it is important to compare Tables 1 and 4, where actual response values are reported for the 2DOF and 6DOF LRB1-isolated building models. The close matches among the reported values must be highlighted. Base drifts match almost perfectly for both models under all input motions, regardless of the presence of higher-mode dynamics; this feature supports the use of simple models (even single-degree-of-freedom superstructure models) as a reasonable tool during early stages of control design. The 2DOF force-displacement loops in Fig. 8 are extremely close to those for the 6DOF (not shown here for brevity). Absolute accelerations are quite comparable, particularly for large seismic scale factors and/or severe earthquake action (Kobe and Northridge), though with slightly less agreement than base drifts. While base acceleration can be compared in a unique way, structure acceleration cannot since the 6DOF model has multiple floors. As one might expect, the structural accelerations reported in Table 1 seem to be comparable to the mean of the second and third floor accelerations reported in Table 4. Finally, interstory drifts (or structural drift) are difficult to compare. The values reported for the 2DOF model are about three times larger than the value corresponding to the first floor of the 6DOF model, and the values decrease with the structure's height. The differences between the 2DOF and 6DOF results in superstructure accelerations and interstory drifts are largely due to the method used to reduce the model to two degrees of freedom; the structure mass in the 2DOF roughly cor-

Table 3. Structural Model Parameters (Kelly et al. 1987)

Floor masses (kg)	Stiffness coefficients (kN/m)	Damping coefficients (kN·s/m)
$m_b = 6800$	$k_b = 232$	$c_b = 3.74$
$m_1 = 5897$	$k_1 = 33732$	$c_1 = 67$
$m_2 = 5897$	$k_2 = 29093$	$c_2 = 58$
$m_3 = 5897$	$k_3 = 28621$	$c_3 = 57$
$m_4 = 5897$	$k_4 = 24954$	$c_4 = 50$
$m_5 = 5897$	$k_5 = 19059$	$c_5 = 38$
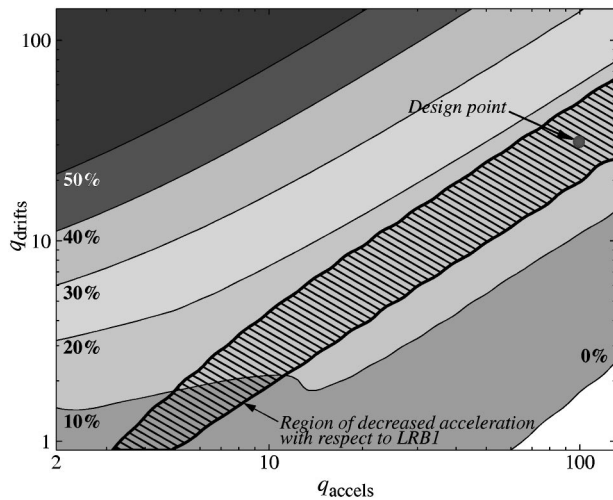
Fig. 11. Regions of smart damper improvement compared to LRB1 baseline

responds to the center-of-gravity of the superstructure, which would be somewhere in the third story of the superstructure. Thus, the 2DOF structure drift corresponds more to the relative displacement of the superstructure center-of-gravity relative to the base; to first order, this drift would be 2–3 times the first story drift.

Second, considering Table 5 and Fig. 12, both LRB2 and smart dampers effectively reduce the base drift compared to the baseline LRB1 design but only the smart damper makes improvements in structural acceleration for most ground motions. Note particularly that the smart damper decreases base drift nearly in half for the strong events (Kobe, Northridge, 2.0×El Centro, 2.0×Hachinohe); LRB2 is slightly less effective for some of the ground motions, but still much better than LRB1. However, peak accelerations, structure interstory drifts, and base shears tell a different story. LRB2 causes peak accelerations to be approximately double the LRB1 design for moderate events, whereas the smart damper is able to achieve good acceleration reductions. Similar reductions in interstory drifts and base shears are

achieved. Consequently, due to its adaptive nature, the smart damper gives good performance for both moderate and severe ground motions.

Concluding Remarks

A "smart" base isolation system, comprised of low-damping elastomeric bearings, and "smart" controllable (semiactive) dampers, was shown to have superior performance compared to several passive base isolation designs using lead-rubber bearings. The peak responses of 2DOF and 6DOF models of a base isolated structure due to several ground motions were computed from simulation. The suite of earthquakes used herein were the 1940 El Centro and 1968 Hachinohe (moderate events) and the 1995 Kobe and 1994 Northridge (severe events) earthquakes. The suite of historical earthquakes were scaled in magnitude to evaluate the base isolation systems during ground motions of different frequency content and various strengths. The responses computed were peak base and structural (relative) displacements, base and structural (absolute) accelerations, applied forces, and base shears. Two lead-rubber bearing designs, denoted LRB1 and LRB2 with bearing yield force Q_y equal to 5 and 15% of the building weight, respectively, were studied. These designs are typical suggestions in the literature for protecting against moderate and strong ground motions, respectively. It was shown herein that the LRB1 system is a near-optimal design for earthquakes of the magnitude and "character" of the 1940 El Centro earthquake, and the LRB2 system is appropriate for strong motions such as the 1994 Northridge or 1995 Kobe earthquakes. A clipped-optimal controller was developed for the smart damper using an H_2/LQG primary controller and a clipping secondary controller to enforce the dissipation requirement. A force saturation limit of 15% of the building weight was imposed to allow a fair comparison with the LRB designs.

The conclusions from both 2DOF and 6DOF studies show that smart dampers can provide superior protection from a wide range of ground motions, whereas the passive lead-rubber bearing designs tend to be suboptimal for events different from their design earthquake. The LRB2 design reduces base drifts compared to the LRB1 design, but only at the expense of significantly larger ac-

Table 4. Peak Drifts (mm), Absolute Accelerations (mg), and Damping Forces (kN) for LRB1 with Six Degree-of-Freedom Model

| Earthquake | PGA (g) | Drift (mm) | | | | | | Acceleration (mg) | | | | | | Base Force (kN) | |
		Base	1st	2nd	3rd	4th	5th	Base	1st	2nd	3rd	4th	5th	Lead	Shear
0.5×El Centro	0.1747	40.8	0.593	0.569	0.449	0.355	0.238	74.9	73.2	69.3	69.3	74.5	78.5	14.37	23.80
1.0×El Centro	0.3495	82.4	0.868	0.855	0.690	0.556	0.380	117.7	112.5	101.1	101.7	114.9	125.1	14.83	33.96
1.5×El Centro	0.5242	167.0	1.334	1.277	1.006	0.793	0.533	159.7	155.7	149.3	155.4	166.6	175.8	14.83	53.67
2.0×El Centro	0.6990	300.5	2.075	1.965	1.531	1.195	0.796	235.1	239.7	239.5	242.2	253.3	262.4	14.83	84.71
0.5×Hachinohe	0.1147	41.9	0.609	0.587	0.464	0.367	0.247	77.5	75.0	69.9	71.2	77.0	81.5	14.63	24.38
1.0×Hachinohe	0.2294	93.2	0.901	0.890	0.723	0.586	0.402	124.5	120.1	110.4	105.0	120.3	132.5	14.83	36.50
1.5×Hachinohe	0.3440	167.9	1.304	1.219	0.960	0.763	0.516	165.4	161.0	151.9	152.2	159.5	170.0	14.83	53.84
2.0×Hachinohe	0.4587	311.2	2.106	1.958	1.497	1.148	0.754	242.1	243.9	245.2	246.0	247.1	248.4	14.83	87.14
0.5×Kobe	0.4168	132.3	1.113	1.046	0.808	0.626	0.414	127.3	128.2	128.5	130.3	133.6	136.5	14.83	45.65
1.0×Kobe	0.8337	265.1	1.884	1.792	1.403	1.107	0.742	232.2	229.8	220.5	219.9	233.1	244.5	14.83	76.44
1.5×Kobe	1.2505	453.6	2.919	2.758	2.146	1.673	1.114	347.7	348.7	343.8	340.6	355.0	366.9	14.83	120.27
0.5×Northridge	0.4214	231.8	1.654	1.559	1.215	0.949	0.633	206.0	203.6	197.6	193.7	201.3	208.5	14.83	68.67
1.0×Northridge	0.8428	556.4	3.519	3.311	2.560	1.985	1.314	412.8	410.8	405.1	410.7	423.2	433.1	14.83	144.07
1.5×Northridge	1.2642	1013.7	6.019	5.603	4.306	3.323	2.194	717.3	716.4	710.2	703.1	711.7	722.8	14.83	250.24

Table 5. Percent Improvement (i.e., Reduction) Compared to LRB1 for Six Degree-of-Freedom Model (Positive Numbers are Better)

Earthquake	PGA (g)	Base Drift			Structural Drift[a]				Base Acceleration			Structural Acceleration[a]				Supplementary Force		Base Shear			
		Smart	LRB2	Rubber	Smart	LRB2	Rubber	Fixed	Smart	LRB2	Rubber	Smart	LRB2	Rubber	Fixed	Smart	LRB2	Smart	LRB2	Rubber	Fixed
0.5×El Centro	0.1747	14.1	3.0	−288.7	35.2	−111.7	−50.0	−604.7	29.6	−99.8	−37.4	26.2	−103.7	−33.6	−662.4	8.4	−194.0	34.8	−116.1	−54.6	−474.6
1.0×El Centro	0.3495	15.1	13.1	−284.4	11.5	−78.7	−104.8	−862.1	10.5	−82.4	−74.7	7.4	−85.0	−67.6	−856.6	−77.6	−218.1	8.6	−88.1	−116.7	−705.3
1.5×El Centro	0.5242	37.1	37.3	−184.7	13.6	−37.9	−99.9	−839.3	1.0	−57.7	−93.2	1.1	−58.5	−79.0	−921.6	−166.4	−222.9	13.2	−34.6	−105.7	−664.5
2.0×El Centro	0.6990	53.4	52.8	−110.9	25.9	−0.6	−71.3	−705.0	10.3	−23.4	−75.0	11.7	−18.7	−59.9	−812.3	−255.2	−223.8	26.7	−73.8	4.4	−545.8
0.5×Hachinohe	0.1147	23.0	15.7	−569.5	48.8	−97.6	−158.6	−447.1	51.7	−80.1	−133.3	48.8	−82.3	−127.1	−547.8	5.6	−181.1	48.2	−102.5	−167.4	−336.4
1.0×Hachinohe	0.2294	30.7	31.1	−502.8	30.8	−70.9	−249.7	−639.9	39.8	−42.5	−190.7	37.0	−50.6	−179.5	−697.2	−86.2	−219.4	30.8	−70.7	−257.2	−483.0
1.5×Hachinohe	0.3440	42.3	41.5	−401.8	28.3	−35.9	−262.4	−666.9	32.1	−42.5	−228.2	26.3	−45.4	−226.5	−831.5	−179.2	−223.7	29.6	−31.6	−263.3	−492.9
2.0×Hachinohe	0.4587	58.5	52.1	−260.9	41.3	1.8	−199.2	−533.1	38.9	−18.2	−198.9	32.8	−22.4	−198.1	−750.3	−260.0	−224.0	42.1	5.1	−199.3	−388.4
0.5×Kobe	0.4168	47.9	24.2	−45.5	15.6	−56.8	2.3	−754.5	19.7	−103.8	4.4	7.2	−114.3	5.6	−989.5	−136.2	−223.6	17.9	1.9	−56.4	−578.1
1.0×Kobe	0.8337	48.4	36.2	−45.3	5.3	−15.4	−15.4	−909.6	6.3	−55.4	−4.9	3.0	−68.9	−5.4	−1116.7	−260.0	−224.0	3.5	−17.2	−14.6	−709.9
1.5×Kobe	1.2505	49.3	26.9	−27.4	19.6	−4.0	−11.7	−877.3	16.2	−26.8	−5.1	8.8	−39.0	−5.3	−1116.2	−260.0	−224.0	21.4	−11.7	−4.2	−672.1
0.5×Northridge	0.4214	45.4	50.6	−109.8	19.4	−9.3	−65.0	−663.1	31.8	−17.1	−51.7	18.8	−22.5	−53.9	−868.1	−210.1	−223.9	21.9	−8.4	−64.4	−489.7
1.0×Northridge	0.8428	46.0	37.9	−74.7	24.3	9.5	−55.1	−617.5	25.6	0.9	−51.4	21.2	−0.3	−48.2	−832.2	−260.0	−224.0	25.4	11.0	−56.7	−462.2
1.5×Northridge	1.2642	42.8	35.4	−43.9	29.8	18.9	−36.0	−529.2	30.7	13.9	−30.7	27.9	12.4	−33.2	−737.8	−260.0	−224.0	30.9	20.0	−35.3	−385.5

[a]These values are the changes in maximums over all stories of the structure; for example, if $d_i(t)$ denotes the interstory drift time history of the ith floor, then the percent improvement is given by $(\max_{i,t}|d_i^{LRB1}(t)| - \max_{i,t}|d_i^{system}(t)|)/\max_{i,t}|d_i^{LRB1}(t)| \times 100\%$, where system denotes the isolation system.
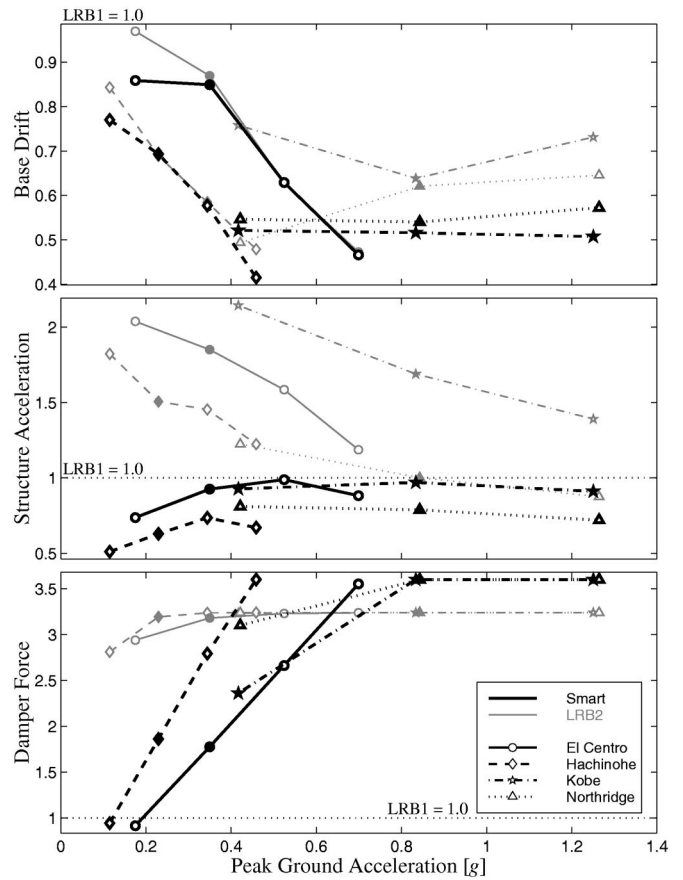
Fig. 12. Peak base drift, structural acceleration, and damper force for the six degree-of-freedom model relative to LRB1. Filled markers denote responses due to unscaled historical earthquakes.

celerations, structural interstory drifts, and base shears in moderate earthquakes compared to the LRB1 design. This trade-off between the various responses is well recognized in the literature, and would be expected with other passive yielding isolation systems (e.g., friction pendulum systems, metallic yielding supplemental dampers) as well. Such large accelerations can damage sensitive equipment or cause damage to nonstructural components, potentially removing the structure and its contents from service. A smart damper, due to its adaptive nature can reduce base drifts as well, and sometimes better, than the LRB2 system while simultaneously reducing structural accelerations, interstory drifts, and base shears. Thus, the adaptable nature of the smart damper system allows a structure to be protected against extreme earthquakes, without sacrificing performance during the more frequent, moderate seismic events. This study suggests that smart dampers, such as magnetorheological fluid dampers, show significant promise for use in base isolation applications.

Acknowledgments

References

Asher, J. W., Young, R. P., and Ewing, R. D. (1996). "Seismic isolation design of the San Bernardino county medical center replacement

project." *J. Struct. Des. Tall Bldgs.,* 5, 265–279.

AASHTO. (1991). "Guide specifications for seismic isolation design." American Association of State Highway and Transportation Officials, Washington, D.C..

Dyke, S. J., Spencer, B. F., Jr., Sain, M. K., and Carlson, J. D. (1996a). "Seismic response reduction using magnetorheological dampers." *Proc., IFAC World Congress*, San Francisco, L:145–150.

Dyke, S. J., Spencer, B. F., Jr., Sain, M. K., and Carlson, J. D. (1996b). "Modeling and control of magnetorheological dampers for seismic response reduction." *Smart Mater. Struct.,* 5, 565–575.

Feng, Q., and Shinozuka, M. (1990). "Use of a variable damper for hybrid control of bridge response under earthquake." *Proc., U.S. National Workshop on Structural Control Research*, USC Publication No. CE-9013.

Hall, J. F., ed. (1995). "Northridge earthquake of January 17, 1994 reconnaissance report." *Earthquake Spectra,* 11, Supplement C, Vol. 1.

Hall, J. F. (1999). "Discussion of 'The role of damping in seismic isolation'." *Earthquake Eng. Struct. Dyn.,* 28, 1717–1720.

Hall, J. F., Heaton, T. H., Halling, M. W., and Wald, D. J. (1995). "Near-source ground motion and its effects on flexible buildings." *Earthquake Spectra,* 11(4), 569–605.

Heaton, T. H., Hall, J. F., Wald, D. J., and Halling, M. V. (1995). "Response of high-rise and base-isolated buildings in a hypothetical Mw 7.0 blind thrust earthquake." *Science,* 267, 206–211.

Inaudi, J. A., and Kelly, J. M. (1993a). "Hybrid isolation systems for equipment protection." *Earthquake Eng. Struct. Dyn.,* 22, 297–313.

Inaudi, J. A., and Kelly, J. M. (1993b). "Optimum damping in linear isolation systems." *Earthquake Eng. Struct. Dyn.,* 22, 583–598.

International Conference of Building Officials (ICBO). (1994). *Uniform building code, earthquake regulations for seismic-isolated structures*, Vol. 2, Appendix Chapt. 16, Whittier, Calif.

International Conference of Building Officials (ICBO). (1997). *Uniform building code, earthquake regulations for seismic-isolated structures*, Vol. 2, Appendix Chapt. 16, Whittier, Calif.

Johnson, E. A., Baker, G. A., Spencer, B. F., Jr., and Fujino, Y. (2003). "Semiactive damping of stay cables." *J. Eng. Mech.*, in press.

Johnson, E. A., Ramallo, J. C., Spencer, B. F., Jr., and Sain, M. K. (1999). "Intelligent base isolation systems." *Proc., 2nd World Conf. on Structural Control*, Kyoto, Japan, Vol. 1, 367–376.

Kelly, J. M. (1997). *Earthquake-resistant design with rubber*, 2nd Ed., Springer, New York.

Kelly, J. M. (1999a). "The role of damping in seismic isolation." *Earthquake Eng. Struct. Dyn.,* 28, 3–20.

Kelly, J. M. (1999b). "The current state of base isolation in the United States." *Proc., 2nd World Conf. on Structural Control*, Kyoto, Japan, Vol. 1, 1043–1052.

Kelly, J. M., Leitmann, G., and Soldatos, A. G. (1987). "Robust control of base-isolated structures under earthquake excitation." *J. Optim. Theory Appl.,* 53, 159–180.

Kelly, J. M., and Tsai, H.-C. (1985). "Seismic response of light internal equipment in base-isolated structures." *Earthquake Eng. Struct. Dyn.,* 13, 711–732.

Kelly, J. M., and Tsai, H.-C. (1993). "Seismic response of heavily damped base isolation systems." *Earthquake Eng. Struct. Dyn.,* 22, 633–645.

Kikuchi, M., and Aiken, I. D. (1997). "An analytical hysteresis model for elastomeric seismic isolation bearings." *Earthquake Eng. Struct. Dyn.,* 26, 215–231.

Kurata, N., Kobori, T., Takahashi, M., Niwa, N., and Hiroshi, M. (1999). "Actual seismic response controlled building with semi-active damper." *Earthquake Eng. Struct. Dyn.,* 28(11), 1427–1447.

Makris, N. (1997). "Rigidity-plasticity-viscosity: Can electrorheological dampers protect base isolated structures from near-source ground motions?" *Earthquake Eng. Struct. Eng.,* 26, 571–591.

Naeim, F., and Kelly, J. M. (1999). *Design of seismic isolated structures: From theory to practice*, Wiley, Chichester, England.

Nagarajaiah, S. (1994). "Fuzzy controller for structures with hybrid isolation system." *Proc., 1st World Conf. on Structural Control*, Los Angeles, TA2, 67–76.

Nagarajaiah, S., Riley, M. A., and Reinhorn, A. (1993). "Control of sliding-isolated bridge with absolute acceleration feedback." *J. Eng. Mech.,* 119(11), 2317–2332.

Nagarajaiah, S., and Xiaohong, S. (2000). "Response of base-isolated USC hospital building in Northridge Earthquake." *J. Struct. Eng.,* 126(10), 1177–1186.

Niwa, N., Kobori, T., Takahashi, M., Matsunaga, Y., Kurata, N., and Mizuno, T. (1999). "Application of semi-active damper system to an actual building." *Proc., 2nd World Conf. on Structural Control*, Kyoto, Japan, Vol. 1, 815–824.

Park, J., and Otsuka, H. (1999). "Optimal yield level of bilinear seismic isolation devices." *Earthquake Eng. Struct. Dyn.,* 28, 941–955.

Reinhorn, A. M., and Riley, M. (1994). "Control of bridge vibrations with hybrid devices." *Proc., 1st World Conf. on Structural Control*, Los Angeles, TA2, 50–59.

Reinhorn, A. M., Soong, T. T., and Wen, C. Y. (1987). "Base-isolated structures with active control." *Proc., ASME PVP Conf.*, San Diego, PVP-127, 413–420.

Schmitendorf, W. E., Jabbari, F., and Yang, J. N. (1994). "Robust control techniques for buildings under earthquake excitation." *Earthquake Eng. Struct. Dyn.,* 23, 539–552.

Skinner, R. I., Robinson, W. H., and McVerry, G. H. (1993). *An introduction to seismic isolation*, Wiley, Chichester, England.

Soong, T. T., and Dargush, G. F. (1997). *Passive energy dissipation systems in structural engineering*, Wiley, New York.

Soong, T. T., and Grigoriu, M. (1993). *Random vibration of mechanical and structural systems*, Prentice-Hall, Englewood Cliffs, N.J.

Spencer, B. F., Jr. (1986). "On the reliability of nonlinear hysteretic structures subjected to broadband random excitation." *Lecture notes in engineering*, C. A. Brebbia and S. A. Orszag, eds., 21, Springer, New York.

Spencer, B. F., Jr., Johnson, E. A., and Ramallo, J. C. (2000). "'Smart' isolation for seismic control." *JSME Int. J., Ser. C,* 43(3), 704–711.

Spencer, B. F., Jr., and Sain, M. K. (1997). "Controlling buildings: A new frontier in feedback." *IEEE Control Syst. Mag.,* 17(6), 19–35.

Symans, M. D., and Constantinou, M. C. (1999). "Semi-active control systems for seismic protection of structures: A state-of-the-art review." *Eng. Struct.,* 21, 469–487.

Symans, M. D., and Kelly, S. W. (1999). "Fuzzy logic control of bridge structures using intelligent semi-active seismic isolation." *Earthquake Eng. Struct. Dyn.,* 28, 37–60.

Taylor, D. P., and Constantinou, M. C. (1996). "Fluid dampers for applications of seismic energy dissipation and seismic isolation." *Tech. Rep.*, Taylor Devices, Inc., North Tonawanda, N.Y. (An updated version of this report is on the web at ⟨http://www.taylordevices.com/dampers.htm⟩).

Wang, Y. P., and Liu, C. J. (1994). "Active control of base-isolated structures under strong earthquakes." *Proc., 5th USA National Conf. on Earthquake Engineering*, Chicago, July 10–14, 1994, Vol. 1, 565–574.

Wen, Y. K. (1976). "Method for random vibration of hysteretic systems." *J. Eng. Mech. Div.,* 102(2), 249–263.

Yang, J. N., Wu, J. C., Reinhorn, A. M., and Riley, M. (1996). "Control of sliding-isolated buildings using sliding-mode control." *J. Struct. Eng.,* 122(2), 179–186.

Yoshida, K., Kang, S., and Kim, T. (1994). "LQG control and H_∞ control of vibration isolation for multi-degree-of-freedom systems." *Proc., 1st World Conf. on Structural Control*, Los Angeles, TP4, 43–52.

Yoshida, K., Yoshida, S., and Takeda, Y. (1999). "Semi-active control of base isolation using feedforward information of disturbance." *Proc., 2nd World Conf. on Structural Control*, Kyoto, Japan, Vol. 1, 377–386.